J|A|C|S
ARTICLES
Published on Web 11/28/2002

Polymeric Nanogels Produced via Inverse Microemulsion Polymerization as Potential Gene and Antisense Delivery Agents

Karen McAllister,[†] Peter Sazani,[‡] Mirielle Adam,[†] Moo J. Cho,[§] Michael Rubinstein,[†] Richard Jude Samulski,[||] and Joseph M. DeSimone*[,†,⊥]

Contribution from the Department of Chemistry, Campus Box 3290, Department of Pharmacology, Campus Box 7295, School of Pharmacy, Campus Box 7360, and Gene Therapy Center, Campus Box 7352, University of North Carolina at Chapel Hill, Chapel Hill, North Carolina 27599, and Department of Chemical Engineering, North Carolina State University, Raleigh, North Carolina 27695

Received July 18, 2002

Abstract: Polymeric nanogel vectors were developed for cellular gene and antisense delivery. Inverse microemulsion polymerization was utilized to synthesize biocompatible nanogels with controlled size, morphology, and composition. The chemical composition, size, polydispersity, stability, and swelling behavior of the nanogels were investigated by NMR, light scattering, transmission electron microscopy, and atomic force microscopy. The cell viability, uptake, and physical stability of nanogel−DNA complexes were evaluated under physiological conditions. Monodisperse nonionic and cationic nanogels were produced with controllable sizes ranging from 40 to 200 nm in diameter. The nanogels demonstrated extended stability in aqueous media and exhibited low toxicity in cell culture. Cationic nanogels formed monodisperse complexes with oligonucleotides and showed enhanced oligonucleotide uptake in cell culture. The nanogels synthesized in this study demonstrate potential utility as carriers of oligonucleotides and DNA for antisense and gene delivery.

Introduction

The advancement of gene and antisense therapies hinges on the implementation of safe and effective delivery systems. Many diseases and cancers are caused by mutations or defects in a single gene.[1] To provide a long-term cure for genetic defects, researchers in the area of gene and antisense therapy are developing methods for gene regulation, repair, and replacement.[1] These methods require insertion of genetic material into the cell nucleus. Several biological barriers prevent injected genetic material from efficiently reaching target cell populations and crossing membranes in vivo.[2−5] A delivery agent, therefore, is required to attain efficient cellular and nuclear uptake of genetic material.[2,3]

Recently, viral and nonviral vectors have been developed for DNA and oligonucleotide delivery. Viral vectors utilize recombinant viruses such as retrovirus,[6] adenovirus,[7] adeno-associated virus,[8] and herpes-simplex virus[9] to package and deliver genes, while nonviral vectors utilize materials such as cationic lipids,[10−12] liposomes,[13,14] surfactants,[15−17] copolymers,[18−22] peptides,[23,24]

* Corresponding author. Telephone: (919) 962-2166. Fax: (919) 962-5467. E-mail: desimone@unc.edu.
[†] Department of Chemistry, University of North Carolina at Chapel Hill.
[‡] Department of Pharmacology, University of North Carolina at Chapel Hill.
[§] School of Pharamcy, University of North Carolina at Chapel Hill.
[||] Gene Therapy Center, University of North Carolina at Chapel Hill.
[⊥] North Carolina State University.

(1) Drew, J.; Martin, L.-A. In *Understanding Gene Therapy*; Lemoine, N. R., Ed.; Springer-Verlag: New York, 1999.
(2) Pouton, C. W.; Seymour, L. W. *Adv. Drug Delivery Rev.* **2001**, *46*, 187−203.
(3) Akhtar, S.; Hughes, M. D.; Khan, A.; Bibby, M.; Hussain, M.; Nawaz, Q.; Double, J.; Sayyed, P. *Adv. Drug Delivery Rev.* **2000**, *44*, 3−21.
(4) Bally, M. B.; Harvie, P.; Wong, F. M. P.; Kong, S.; Wasan, E. K.; Reimer, D. L. *Adv. Drug Delivery Rev.* **1999**, *38*, 291−315.
(5) Takakura, Y.; Mahato, R. I.; Hashida, M. *Adv. Drug Delivery Rev.* **1998**, *34*, 93−108.
(6) Cannon, P. M.; Anderson, W. F. In *Gene Therapy: Therapeutic Mechanisms and Strategies*; Templeton, N. S., Lasic, D. D., Eds.; Marcel Dekker: New York, 2000.
(7) Hackett, N. R.; Crystal, R. G. In *Gene Therapy: Therapeutic Mechanisms and Strategies*; Templeton, N. S., Lasic, D. D., Eds.; Marcel Dekker: New York, 2000.
(8) Monahan, P. E.; Samulski, R. J. *Mol. Med. Today* **2000**, *6*, 433−440.
(9) Wolfe, D.; Goins, W. F.; J., F. D.; Glorioso, J. C. I. In *Gene Therapy: Therapetuic Mechanisms and Strategies*; Templeton, N. S., Lasic, D. D., Eds.; Marcel Dekker: New York, 2000.
(10) Zelphati, O.; Szoka, F. C. J. *Pharm. Res.* **1996**, *13*, 1367−1372.
(11) Xu, Y.; Hui, S.-W.; Frederik, P.; Szoka, F. C. J. *Biophys. J.* **1999**, *77*, 341−353.
(12) Birchall, J. C.; Kellaway, I. W.; Mills, S. N. *Int. J. Pharm.* **1999**, *183*, 195−207.
(13) Pedroso de Lima, M.; Simoes, S.; Pires, P.; Gaspar, R.; Slepushkin, V.; Duzgunes, N. *Mol. Membr. Biol.* **1999**, *16*, 103−109.
(14) Choi, J. S.; Lee, E. J.; Jang, H. S.; Park, J. S. *Bioconjugate Chem.* **2001**, *12*, 108−113.
(15) McGregor, C.; Perrin, C.; Monck, M.; Camilleri, P.; Kirby, A. J. *J. Am. Chem. Soc.* **2001**, *123*, 6217−6220.
(16) Dauty, E.; Remy, J.-S.; Blessing, T.; Behr, J.-P. *J. Am. Chem. Soc.* **2001**, *123*, 9227−9234.
(17) Ouyang, M.; Remy, J.-S.; Szoka, F. C. J. *Bioconjugate Chem.* **2000**, *11*, 104−112.
(18) Kataoka, K.; Harada, A.; Nagasaki, Y. *Adv. Drug Delivery Rev.* **2001**, *47*, 113−131.
(19) Kabanov, A. V.; Kabanov, V. A. *Adv. Drug Delivery Rev.* **1998**, *30*, 49−60.
(20) Vinogradov, S. V.; Bronich, T. K.; Kabanov, A. V. *Bioconjugate Chem.* **1998**, *9*, 805−812.

10.1021/ja027759q CCC: $22.00

polycations,[25] polymeric particles,[23,26−32] dendrimers,[33,34] and cyclodextrins[35,36] to condense[37,38] and deliver oligonucleotides and DNA. Although many of these delivery systems have been evaluated in vivo and are discussed in numerous reviews,[19,39−47] no system currently provides the efficacy, safety, and formulation stability required for clinical use. A vector must resist premature enzymatic degradation and aggregation in vivo, target specific tissues, cross the cell membrane, facilitate nuclear uptake, and provide controlled release of the genetic material, while not inducing toxicity or an immune response.[2,4] For in vivo applications, vectors of sizes below 200 nm in diameter are desired for systemic circulation,[2,4,5] and monodisperse vectors, homogeneous in size and composition, are preferred to enable pharmacokinetic analysis of a single active species.

To address the issues of poor stability, large size, and heterogeneity[41] associated with many nonviral vectors, this research has utilized the synthetic method, inverse microemulsion polymerization, to design stable, monodisperse, and biocompatible polymeric nanogels of sizes below 200 nm for cellular delivery of DNA and oligonucleotides. Such polymeric materials may offer potential utility as in vivo carriers of DNA and oligonucleotides and can be further designed and optimized to target specific cells and promote controlled release and nuclear uptake.

Previously, microemulsion polymerization has been employed to produce polymeric particles or gels with narrow size distributions and spherical morphologies.[48−52] Several researchers have exploited inverse microemulsion polymerization to prepare submicrometer, nonionic, hydrophilic particles for protein and enzyme delivery systems.[53−58] An inverse microemulsion contains water-swollen surfactant micelles dispersed in a continuous oil phase.[59] Free radical polymerization of monomers dissolved in these water-swollen micelles often results in monodisperse polymer particles of sizes less than 1 μm.[48,60,61] The small particle sizes and narrow size distributions obtained from inverse microemulsion polymerization make this method attractive for the preparation of nanogels designed to form monodisperse complexes with DNA.

Recently, Vinogradov, Bronich, and Kabanov reported the preparation of crosslinked poly(ethylene glycol)-*cl*-polyethyleneimine particles using a modified emulsification/solvent evaporation method.[62] The size distribution of these networks ranged between 40 and 300 nm, and the networks formed complexes with negatively charged oligonucleotides and enhanced the uptake of oligonucleotides in cell culture.[62] Inverse microemulsion polymerization is expected to obtain crosslinked networks having similar properties but with narrower size distributions.

This article details the synthesis and characterization of polymeric nanogels produced via inverse microemulsion polymerization. The chemical composition, size, polydispersity, stability, swelling behavior, and toxicity of the nanogels were investigated, and nanogel−DNA complexes were prepared and assayed in vitro to determine the morphology, physical stability, and cellular distribution of the complexes. The results presented provide insight into the experimental and synthetic conditions required to develop effective nanogel vectors.

Results and Discussion

Inverse Microemulsion Polymerization. The following acrylate monomers were polymerized in inverse microemulsions to produce hydrophilic nanogels: 2-acryloxyethyltrimethylammonium chloride (AETMAC), 2-hydroxyethylacrylate (HEA), and poly(ethylene glycol)diacrylate (PEGdiA). These monomers are water-soluble and possess similar reactivity toward free radical polymerization. The quaternary ammonium ion monomer, AETMAC, was selected to promote pH-independent condensation of DNA via electrostatic association between the phosphate groups and quaternary ammonium ion side chains.

(21) Lim, D. W.; Yeom, Y. I.; Park, T. G. *Bioconjugate Chem.* **2000**, *11*, 688−695.
(22) Toncheva, V.; Wolfert, M. A.; Dash, P. R.; Oupicky, D.; Ulbrich, K.; Seymour, L. W.; Schact, E. H. *Biochim. Biophys. Acta* **1998**, *1380*, 354−368.
(23) Junghans, M.; Kreuter, J.; Zimmer, A. *Biochim. Biophys. Acta* **2001**, *1544*, 177−188.
(24) Adami, R. C.; Collard, W. T.; Gupta, S. A.; Kwok, K. Y.; Bonadio, J.; Rice, K. G. *J. Pharm. Sci.* **1998**, *87*, 678−683.
(25) Bettinger, T.; Remy, J.-S.; Erbacher, P. *Bioconjugate Chem.* **1999**, *10*, 558−561.
(26) Aynie, I.; Vauthier, C.; Chacun, H.; Fattal, E.; Couvreur, P. *Antisense Nucleic Acid Drug Dev.* **1999**, *9*, 301−312.
(27) Berton, M.; Benimetskaya, L.; Allemann, E.; Stein, C. A.; Gurny, R. *Eur. J. Pharm. Biopharm.* **1999**, *47*, 119−123.
(28) Fattal, E.; Vauthier, C.; Aynie, I.; Nakada, Y.; Lambert, G.; Malvy, C.; Couvreur, P. *J. Controlled Release* **1998**, *53*, 137−143.
(29) Berton, M.; Turelli, P.; Trono, D.; CStein, C. A.; Allemann, E.; Gurnay. *Pharm. Res.* **2001**, *18*, 1096−1101.
(30) Coester, C.; Kreuter, J.; von Briesen, H.; Langer, K. *Int. J. Pharm.* **2000**, *196*, 147−149.
(31) Vinogradov, S. V.; Batrakova, E.; Kabanov, A. V. *Colloids Surf. B: Biointerfaces* **1999**, *16*, 291−304.
(32) Zobel, H. P.; Stieneker, F.; Aziz, S. A.-A.; Gilbert, M.; Werner, D.; Noe, C. R.; Kreuter, J.; Zimmer, A. *Eur. J. Pharm. Biopharm.* **1999**, *48*, 1−12.
(33) Tang, M. X.; Redemann, C. T.; Szoka, F. C. J. *Bioconjugate Chem.* **1996**, *7*, 703−714.
(34) Lim, Y.-b.; Kim, S.-M.; Lee, Y.; Lee, W.-k.; Yang, T.-g.; Lee, M.-j.; Suh, H.; Park, J.-s. *J. Am. Chem. Soc.* **2001**, *123*, 2460−2461.
(35) Redenti, E.; Pietra, C.; Gerloczy, A.; Szente, L. *Adv. Drug Delivery Rev.* **2001**, *53*, 235−244.
(36) Hwang, S. J.; Bellocq, N. C.; Davis, M. E. *Bioconjugate Chem.* **2001**, *12*, 280−290.
(37) Bloomfield, V. A. *Curr. Opin. Struct. Biol.* **1996**, *6*, 334−341.
(38) Bloomfield, V. A. *Biopolymers* **1998**, *44*, 269−282.
(39) Smith, L. C.; Duguid, J.; Wadhwa, M. S.; Logan, M. J.; Tung, C.-H.; Edwards, V.; Sparrow, J. T. *Adv. Drug Delivery Rev.* **1998**, *30*, 115−131.
(40) Pichon, C.; Goncalves, C.; Midoux, P. *Adv. Drug Delivery Rev.* **2001**, *53*, 75−94.
(41) Garnett, M. C. *Crit. Rev. Ther. Drug Carrier Syst.* **1999**, *16*, 147−207.
(42) Kabanov, A. V. *Pharm. Sci. Technol. Today* **1999**, *2*, 365−372.
(43) Rolland, A. P. *Crit. Rev. Ther. Drug Carrier Syst.* **1998**, *15*, 142−198.
(44) Zuber, G.; Daughty, E.; Nothisen, M.; Belguise, P.; Behr, J.-P. *Adv. Drug Delivery Rev.* **2001**, *52*, 245−253.
(45) Luo, D.; Slaltzman, W. M. *Nature Biotechnol.* **2000**, *18*, 33−37.
(46) Han, S.-o.; Mahato, R. I.; Sung, Y. K.; Kim, S. W. *Mol. Therapy: J. Am. Soc. Gene Therapy* **2000**, *2*, 302−317.
(47) Lambert, G.; Fattal, E.; Courvreur, P. *Adv. Drug Delivery Rev.* **2001**, *47*, 99−112.
(48) Candau, F. In *Soft Matter Physics*; Daoud, M., Williams, C. E., Eds.; Springer: New York, 1995.
(49) Antonietti, M.; Bremser, W.; Schmidt, M. *Macromolecules* **1990**, *23*, 3796−3805.
(50) Antonietti, M. *Macromol. Symp.* **1995**, *93*, 213−225.
(51) Antonietti, M.; Pakula, T.; Bremser, W. *Macromolecules* **1995**, *28*, 4227−4233.
(52) Antonietti, M. *Angew. Chem., Int. Ed. Engl.* **1988**, *27*, 1743−1747.
(53) Daubresse, C.; Grandfils, C.; Jerome, R.; Teyssie, P. *J. Colloid Interface Sci.* **1994**, *168*, 222−229.
(54) Daubresse, C.; Grandfils, C.; Jerome, R.; Teyssie, P. *Colloid Polym. Sci* **1996**, 1996.
(55) Maitra, A.; Ghosh, P. K.; De, T. K.; Sahoo, S. K. In: United States, 1997.
(56) Gupta, A. K.; Madan, S.; Majumdar, D. K.; Maitra, A. *Int. J. Pharm.* **2000**, *209*, 1−14.
(57) Gaur, U.; Sahoo, S. K.; De, T. K.; Ghosh, P. C.; Maitra, A.; Ghosh, P. K. *Int. J. Pharm.* **2000**, *202*, 1−10.
(58) Madan, T.; Munshi, N.; De, T. K.; Maitra, A.; Sarma, P. U.; Aggarwal, S. S. *Int. J. Pharm.* **1997**, *159*, 135−147.
(59) Nagarajan, R.; Ruckenstein, E. *Langmuir* **2000**, *16*, 6400−6415.
(60) Candau, F.; Leong, Y. S.; Fitch, R. M. *J. Polym. Sci.: Polym. Chem. Ed.* **1985**, *23*, 193−214.
(61) Candau, F.; Collin, D.; Kern, F. *Makromol. Chem., Macromol. Symp.* **1990**, *35/36*, 105−119.
(62) Vinogradov, S. V.; Bronich, T. K.; Kabanov, A. V. *Adv. Drug Delivery Rev.* **2002**, *54*, 135−147.

Table 1. Monomer Weight Ratios, Reported as Weight Percent with Respect to Total Monomer Weight, Utilized in Inverse Microemulsion Polymerizations[a]

(A) nonionic P:A:H (wt %)	(B) cationic P:A:H (wt %)	(C) cationic P:A:H (wt %)
3:0:97	3:12:85	3:25:72
6:0:94	6:12:82	6:25:69
12:0:88	12:12:76	12:25:63
24:0:76	24:12:64	24:25:51
50:0:50	50:12:38	50:25:25

[a] P = PEGdiA (crosslinker), A = AETMAC (charged monomer), H = HEA.

Previous studies of linear polymers containing quaternary ammonium ion side chains have illustrated that these cationic polymers are able to facilitate pH-independent condensation of DNA; however, many of these species have exhibited toxicity in cell culture.[32,63,64] Since the toxicity of macromolecules is often influenced by cation content,[41] AETMAC was copolymerized with the nonionic crosslinker PEGdiA and nonionic monomer HEA to prepare nanogels with reduced quaternary ammonium ion content and to determine the minimum level of AETMAC needed to condense DNA without inducing toxicity in cell culture. In addition to lessening the quaternary ammonium ion concentration, PEGdiA was selected to impart biocompatibility, solubility, and stability in physiological media. Many poly(ethylene glycol) derivatives have been utilized extensively in vivo applications to improve the biocompatibility, solubility, stability, and circulation time of proteins, liposomes, and particles.[65,66]

To systematically study the effects of monomer composition on nanogel properties, a series of nanogels ranging in crosslinker and quaternary ammonium ion concentration were synthesized via inverse microemulsion polymerization. Table 1 lists the monomer weight ratios utilized to prepare a series of nonionic and cationic nanogels.

For each reaction condition, a one-phase, optically transparent inverse microemulsion was formed by combining heptane, aqueous monomer solution, and the surfactant laureth-3 in the weight ratios of 86.8/3.5/9.7. Using this ratio of heptane, aqueous phase, and surfactant enabled inverse microemulsions to be attained for all monomer compositions studied. The microemulsions consisted of surfactant micelles swollen with aqueous solutions of monomer dispersed in heptane. Upon polymerization, the monomers inside the micelles reacted and formed polymeric nanogels, surrounded by surfactant. Figure 1 schematically depicts the inverse microemulsion polymerization of monomer-swollen micelles.

For the reactions listed in Table 1, the monomer conversion and composition within the polymer product were determined by proton NMR. Polymerizations, conducted in deuterated solvents and monitored by ^{1}H NMR, did not display signals from unreacted vinylic protons post reaction, indicating monomer conversions of at least 99% were obtained. After polymerization, the polymeric nanogels were isolated in water, and

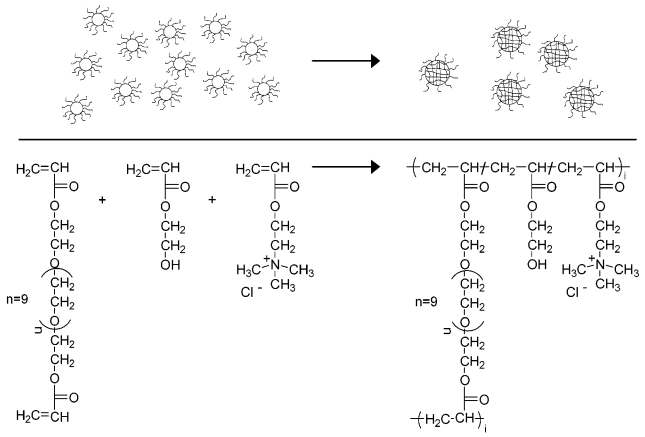

Figure 1. (Top) Schematic representation of monomer-swollen micelles reacting to form polymeric nanogels. (Bottom) The chemical structures of monomers inside micelles and the partial structure of a cationic nanogel.

the heptane and surfactant were removed by extraction and dialysis. Residual heptane, surfactant, and monomer proton signals were not detected in the NMR spectra of purified nanogels. The weight ratios of monomers in the polymer product, calculated from integrating ^{1}H NMR spectra, corresponded closely to the ratios charged into the reaction (data contained in the Supporting Information). As described below, variations in the monomer compositions significantly impacted the nanogel properties including the size, morphology, swelling behavior, interaction with DNA, and uptake in cells.

Light Scattering Analysis of Nanogels. The polymerizations were monitored by dynamic light scattering to determine if submicrometer nanogels were obtained and to measure the influence of crosslinker and charged monomer concentration on the nanogel size, polydispersity, and swelling.

Figure 2 summarizes the hydrodynamic diameters of the micelles in the microemulsions, of the nanogels in the polymerized microemulsions, and of the nanogels in water for the reaction compositions given in Table 1.

In Figure 2, the polymerized nanogels dispersed in heptane appear 2−3 times larger than the initial monomer swollen micelles. It is likely that the increase in diameter is attributable to micelle collisions occurring during free radical polymerization producing a nanogel comprised of multiple reacted monomer micelles. This hypothesis is consistent with mechanistic models reported in the literature for inverse microemulsion polymerization of monomers that do not partition into the continuous phase.[60,67−71] In this mechanism, the primary locus of free radical polymerization is within the monomer-swollen micelles and not in the continuous phase, and the mass of the final particle corresponds to the volume increase multiplied by the mass of the original droplet.

Swelling Studies. Comparison of the hydrodynamic diameters measured in polymerized microemulsion versus water, as depicted in Figure 2, illustrates the influence of the solvent

(63) Zobel, H. P.; Zimmer, A.; Aziz, S. A.-A.; Gilbert, M.; Werner, D.; Noe, C. R.; Kreuter, J.; Stieneker, F. *Eur. J. Pharm. Biopharm.* **1999**, *47*, 203−213.
(64) Wolfert, M. A.; Dash, P. R.; Nazarova, O.; Oupicky, D.; Seymour, L. W.; Smart, S.; Strohalm, J.; Ulbrich, K. *Bioconjugate Chem.* **1999**, *10*, 993−1004.
(65) Woodle, M. C. *Adv. Drug Delivery Rev.* **1998**, *32*, 139−152.
(66) Papisov, M. I. *Adv. Drug Delivery Rev.* **1998**, *32*, 119−138.
(67) Candau, F. *Makromol. Chem., Macromol. Symp.* **1990**, *31*, 27−40.
(68) Medizabal, E.; J., F.; F. E., P.; Lopez-Serrano, F.; Alvarez, J. *Eur. Polym. J.* **1998**, *34*, 411−420.
(69) Morgan, J. D.; Lusvardi, K. M.; Kaler, E. W. *Macromolecules* **1997**, *30*, 1897−1905.
(70) De Buruaga, A. S.; De Le Cal, J.; Asua, J. M. *J. Polym. Sci., Part A: Polym. Chem.* **1999**, *37*, 2167−2178.
(71) De Buruaga, A. S.; Capek, I.; De Le Cal, J.; Asua, J. M. *J. Polym. Sci., Part A: Polym. Chem.* **1998**, *36*, 737−748.

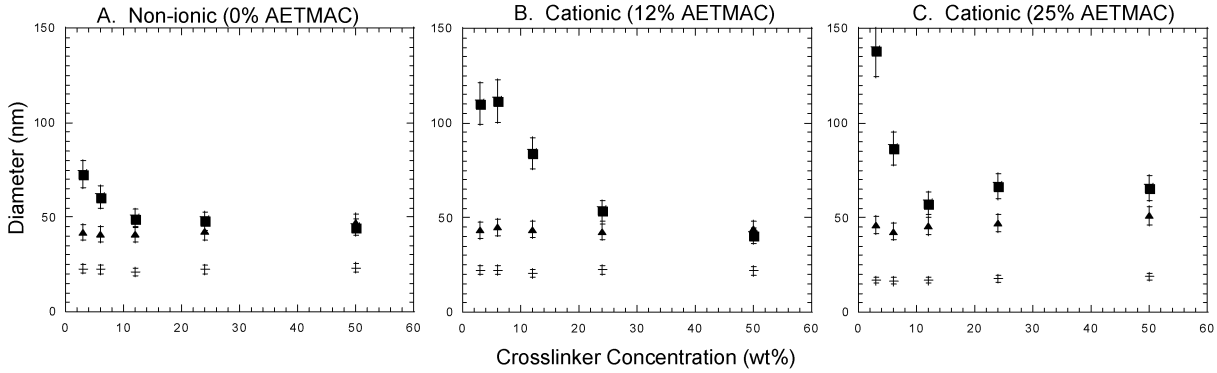

Figure 2. Hydrodynamic diameters of micelles and nanogels vs crosslinker concentration: micelles in microemulsion (+), nanogels in microemulsion (▲), and nanogels in water (■).

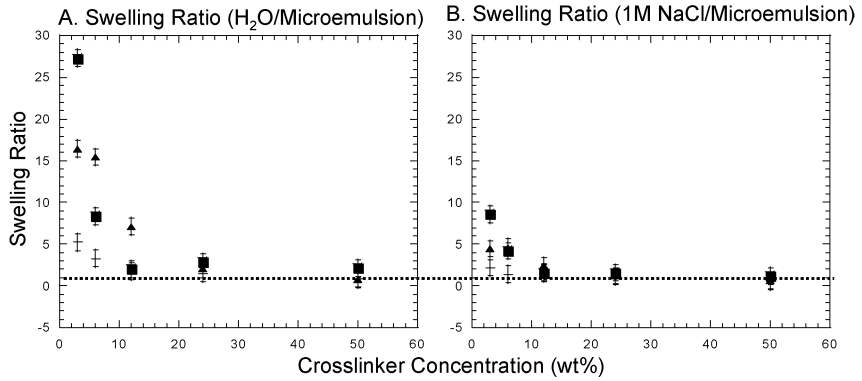

Figure 3. (A) Swelling ratio of nanogels in water vs heptane microemulsion (B). Swelling ratio of nanogels in 1 M NaCl vs heptane microemulsion: nonionic nanogels (+), cationic nanogels with 12 wt % AETMAC (▲), and cationic nanogels with 25 wt % AETMAC (■). Dotted line defines swelling ratio = 1.

environment on the hydrodynamic diameter. In the heptane continuous phase, the sizes were found to be independent of the crosslinker concentration in the monomer phase, suggesting that, in the heptane continuous phase, the nanogels are not fully swollen. This behavior is attributable to heptane being a poor solvent for these polymers, and in order to minimize unfavorable enthalpic interactions, the polymer network does not swell. As expected, removal of the heptane and placement of the nanogels into water, a good solvent, induced swelling. In water, the swelling was controlled by several factors: the crosslinker concentration, charge concentration, and ionic strength. The swelling ratios of the nanogels in aqueous solutions versus in the heptane microemulsions are depicted in Figure 3. The swelling ratios are calculated from the hydrodynamic volumes, as defined by eq 1 D_h = hydrodynamic diameter.

$$\text{swelling ratio} = \frac{(D_{\text{h aqueous solution}})^3}{(D_{\text{h heptane microemulsion}})^3} \qquad (1)$$

As shown in Figure 3A, the nanogels swelled as the crosslinker concentration was decreased, and the cationic nanogels containing the charged monomer, AETMAC, swelled more than the nonionic nanogels. The increased swelling of the cationic nanogels was due to both the osmotic pressure of the counterions and electrostatic repulsions between neighboring charged monomers causing the chains to stretch.[72] Raising the ionic strength of the solution caused the cationic nanogels to deswell, as the surface charges on the nanogels were screened by surrounding solvent ions. This effect has been observed in other polyelectrolyte gel systems.[72] In Figure 3B, when the charges were screened, at the ionic strength of 1 M, the swelling ratios of the charged nanogels corresponded closely to the swelling ratios of the nonionic nanogels at 0 M ionic strength, indicating that at high ionic strengths, the swelling was governed by the crosslinker concentration, and at low ionic strengths the swelling was influenced by both the crosslinker and charge concentration. In both figures, the swelling ratios decreased at high crosslinker concentrations.

Swelling was also investigated in the temperature range of 19−50 °C, and within this temperature range the sizes remained constant, suggesting that the polymers remained in a good solvent regime and did not approach or cross the theta (θ) temperature where deswelling would occur.

These swelling studies demonstrate how nanogels of sizes ranging from 40 to 200 nm can easily be obtained through variations in the monomer compositions. For delivery applications, nanogels, of a specific size, can be designed by selecting the appropriate amount of crosslinker and charged monomer concentration in the polymerization.

Polydispersity Measurements. The size distribution of the nanogels was also evaluated by dynamic light scattering measurements. The nanogels in polymerized microemulsions and in water were probed at scattering angles ranging from 30° to 150°. For these systems, the polydispersity was evaluated by taking the ratio of the diffusion coefficients obtained at the

(72) Rubinstein, M.; Colby, R. H.; Dobrynin, A. V.; Joanny, J.-F. *Macromolecules* **1996**, *29*, 398−406.

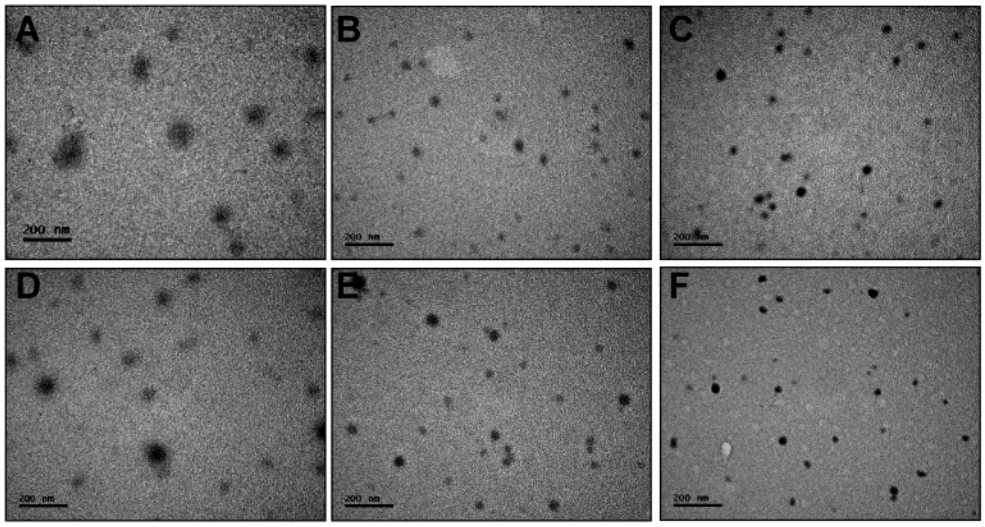

Figure 4. Transmission electron micrographs of nanogels. Nonionic nanogels with PEGdiA:AETMAC:HEA wt ratios 3:0:97 (A), 12:0:88 (B), 50:0:50 (C). Cationic nanogels with PEGdiA:AETMAC:HEA wt ratios 3:12:83 (D), 12:12:76 (E), 50:12:38 (F). Bars = 200 nm.

Table 2. Diffusion Coefficient Ratios for Nanogels in Microemulsions and for Nanogels in Water

PEGdiA (wt %)	(A) nonionic (0 wt % AETMAC)		(B) cationic (12 wt % AETMAC)		(C) cationic (25 wt % AETMAC)	
	M	H	M	H	M	H
3	0.95	0.99	1.01	1.19	0.94	1.34
6	1.00	0.95	0.96	1.18	0.96	1.09
12	0.94	0.94	0.99	1.18	0.96	0.97
24	0.96	0.99	0.98	0.94	1.03	1.05
50	0.96	0.93	1.07	0.94	0.95	1.06

[a] M = microemulsion, H = H_2O.

scattering angle of 150° and extrapolated to $q = 0$, as defined by eq 2.

$$\text{diffusion coefficient ratio} = \frac{D_{q150}}{D_{0q}} \qquad (2)$$

D_{q150}= diffusion coefficient obtained at 150°; D_{0q} = diffusion coefficient extrapolated to $q = 0$. Monodisperse populations, with q independent diffusion coefficients, should possess a ratio equal to 1. Table 2 lists the diffusion coefficient ratios obtained for the nanogels in polymerized microemulsions and for nanogels in water.

The diffusion coefficients obtained for the nonionic nanogels and cationic nanogels in the polymerized microemulsions were q independent, and the values remained within 10% over the range of scattering vectors probed, indicating both the nonionic and cationic nanogels had narrow size distributions in the polymerized microemulsions. When placed into water, the nonionic nanogels and the highly crosslinked cationic nanogels also exhibited q independent diffusion coefficients, indicative of low polydispersity. An increase in polydispersity, however, was observed for the cationic nanogels containing low crosslinker concentrations when analyzed in water versus when analyzed in the heptane microemulsions. As reported in Table 2, the diffusion coefficients for the cationic nanogels containing low crosslinker concentrations in water varied more than 10% over the range of scattering vectors probed. This slight increase in polydispersity may be attributed to heterogeneities in the crosslinker and charge distribution within the sample, affecting the swollen size in water but not affecting the collapsed size in heptane microemulsion, resulting in narrow size distributions in the polymerized microemulsion and slightly broader size distributions in water. This would also explain why, at high crosslinker concentrations, the nanogels in heptane and the nanogels in water both had similar narrow size distributions, because at these crosslinking levels, variations in the crosslinker distribution would not significantly affect the swollen size.

Table 3. Particle Size Analysis of Nonionic and Cationic Nanogels Measured by TEM[a]

PEGdiA (wt %)	nonionic nanogels (nm) (0 wt % AETMAC)	cationic nanogels (nm) (12 wt % AETMAC)
3	81	72
12	45	49
50	38	29

[a] Sizes represent the average size of 50 particles.

Nanogel Stability. The stability of nanogels in aqueous media was monitored by dynamic light scattering. In order for these systems to possess therapeutic utility, they must not aggregate under physiological conditions. Samples were measured after 1 month storage at ambient temperature and after 6 months storage at 4 °C, and for these samples, no change in size or polydispersity was observed.

Microscopy Studies. The morphology of the nanogels was probed by transmission electron microscopy (TEM) and atomic force microscopy (AFM). When the nanogels were dried onto a surface, they were found to possess a flattened spherical morphology. Figure 4 depicts the TEMs of nonionic and cationic nanogels as a function of crosslinker concentration.

By TEM, the sizes were determined and were found to be influenced by the crosslinker concentration; the nanogels with 3 wt % crosslinker (micrographs A and D) appeared larger than the nanogels at higher crosslinker percentages (micrographs B, C, E, and F). Table 3 lists the average sizes of the nanogels depicted in Figure 4.

As the crosslinker concentration decreased, the nanogels were able to flatten more on the surface, thus appearing larger by TEM. In addition, the cationic nanogels, when measured by TEM, were slightly smaller than the nonionic nanogels. This may suggest that the conformation of the nanogels on a surface

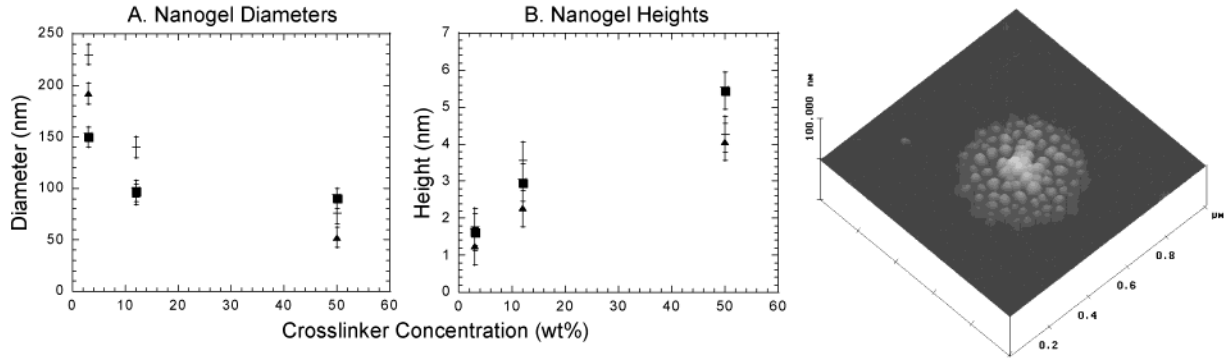

Figure 5. AFM analysis of nanogels. (A) Diameter vs crosslinker concentration, (B) Height vs crosslinker concentration: nanogels with 0 wt % AETMAC (+), 12 wt % AETMAC (▲), and 25 wt % AETMAC (■). (Micrograph) Three-dimensional height image (1 μm × 1 μm × 30 nm) of nanogels prepared with 12 wt % AETMAC and 50 wt % crosslinker on the surface of mica.

is influenced by the crosslinker concentration and not by the charged monomer concentration, unlike the swelling of the nanogels in water, Figure 3A, which was controlled by both the crosslinker and the charged monomer concentration.

To further investigate the flattening of nanogels on a surface, AFM analysis was performed, which provided measurement of both the height and the diameter of the nanogels adsorbed onto a surface. Figure 5 depicts graphs detailing the height and diameter of nanogels as a function of crosslinker concentration and a representative atomic force micrograph of cationic nanogels absorbed unto mica. The clustering of nanogels on the surface of mica in the micrograph is an artifact resulting from spin-coating deposition followed by drying and does not reflect the behavior in solution. By AFM, the measured heights and diameters are respectively smaller and broader than the actual dimensions, presumably due to interactions between the AFM tip and the nanogels. Because of these interactions, the graphical values in Figure 5 provide only a qualitative trend of the dimensions of nanogels deposited on a surface. According to the trends observed from the AFM data, and in agreement with the TEM measurements, the diameter increased and the height decreased as the crosslinker concentration was lowered. This spreading as a function of decreasing crosslinker concentration correlates to the swelling of nanogels in water observed by light scattering and typifies the behavior of soft, low T_g, crosslinked materials adsorbed onto a surface.

The combination of light scattering, transmission electron microscopy, and atomic force microscopy analysis, presented in Figures 2−5, indicates that the nanogels are within the appropriate size range, are resistant to aggregation, and possess low polydispersity for potential utility as gene and antisense vectors. In order for the nanogels to have application as gene and antisense carriers, the nanogels must be able to condense DNA into monodisperse, submicrometer complexes under physiological conditions. DNA−nanogel complexes were prepared and consequently investigated by electrophoresis, chromatography, light scattering, and atomic force microscopy to measure the size and stability of the complexes as a function of the nanogel composition and to determine which compositions would be suitable for potential gene and antisense applications.

Electrophoresis Studies of DNA Complexes. Electrophoresis was performed on nanogels in the presence of DNA, to investigate which nanogel compositions bind to oligonucleotides and DNA. Electrophoresis was performed at varying quaternary

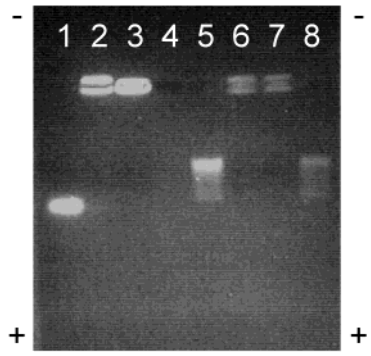

Figure 6. A 1% agarose gel photographed under UV transilluminator. Lanes 1−3: 24 bp fluorescein-labeled DNA + nanogels respectively containing 0, 12, and 25 wt % AETMAC. Lane 4: blank. Lanes 5−7: 100−1000 bp fluorescein-labeled DNA ladder + nanogels respectively containing 0, 12, and 25 wt % AETMAC. Lane 8: control 100−1000 bp fluorescein-labeled DNA. Approximate quaternary ammonium ion/phosphate (N/P) ratios for nanogel−DNA complexes containing 0, 12, and 25 wt % AETMAC are 0:1, 5:1, and 10:1, respectively, and the nanogel concentration is 0.37 mg/mL.

ammonium ion/phosphate (N/P) ratios. The (N/P) ratio defines the ratio of quaternary ammonium ions within the nanogels and the phosphate ions within the DNA. The results of the electrophoresis study indicate that the cationic nanogels containing 12 and 25 wt % AETMAC bind DNA in the presence of an electric field at an ionic strength of 41 mM and at (N/P) ratios of 5:1 and 10:1, respectively. A representative 1% agarose gel is depicted in Figure 6. In this gel, migration of DNA toward the anode occurred in wells containing the nonionic nanogels, while the migration of DNA in the wells containing the cationic nanogels was inhibited, an indication of DNA binding to the cationic nanogels.

To further study the binding of complexes as a function of ionic strength and to determine the size and polydispersity of the complexes in the absence of an electric field, size exclusion chromatography and light scattering measurements were performed.

Size Exclusion Chromatography Study of DNA Complexes. Complex binding at varying ionic strengths was evaluated by size exclusion chromatography. In these experiments, aqueous solutions of nanogels and fluorescein-labeled 24 bp DNA were passed through size exclusion columns at ionic strengths ranging from 10 to 1010 mM. Nanogels and associated DNA eluted through the column prior to unbound oligonucleotides. Under the conditions studied, the nonionic nanogels did

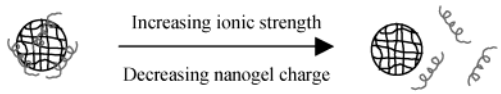

Type	Non-ionic	Cationic	Cationic
Ionic Strength	0% Charge	12% Charge	25% Charge
10 mM	-	+	+
110 mM	-	-	+
1010 mM	-	-	-

Figure 7. (Top) Schematic representation of the influence of ionic strength on the nanogel−DNA complex. (Bottom) Summary of DNA binding to nanogels as a function of ionic strength and nanogel charge: binding (+); no binding (−). Approximate (N/P) ratios for nanogel−oligonucleotide complexes containing 0, 12, and 25 wt % AETMAC (charge) are 0:1, 100:1, and 200:1, respectively.

Table 4. Diameter and Diffusion Coefficient Ratio of Nanogel−DNA Complexes in 1X PBS As Determined by Dynamic Light Scattering[a]

sample	diameter (nm)	diff coeff ratio
nanogels without DNA	55	1.05
nanogels + 24 bp DNA (N/P) 10:1	56	1.09
nanogel + 1000 bp DNA (N/P) 10:1	740	5.04

[a] The nanogel concentration is 0.125 mg/mL, and the nanogel composition is PEGdiA:AETMAC:HEA weight ratio of 12:25:63.

not bind DNA, while the cationic nanogels complexed to DNA. The formation of complexes depended on the ionic strength and nanogel charge. Figure 7 summarizes the chromatographic conditions studied and the ionic strengths that the nanogel−DNA complexes actually formed.

According to the chromatography results, complexes were not formed with nanogels containing 0 and 12 wt % AETMAC at physiological ionic strength; however, complexes did form with nanogels containing 25 wt % AETMAC at 110 mM and at physiological ionic strength of 150 mM. The formation of complexes was reversible, and at ionic strengths of 1 M, all the complexes dissociated. This suggests that for in vivo applications where complexes must form at physiological ionic strength, nanogels with AETMAC concentrations exceeding 12 wt % are required.

Size and Stability of Complexes. Although the nanogels containing 25 wt % AETMAC were able to complex DNA under physiological conditions, it was critical to determine if the complexes were stable, were submicrometer sized, and possessed low polydispersity. The stability, morphology, and polydispersity of the DNA−nanogel complexes were investigated by light scattering and AFM. To determine the size and polydispersity of the complexes, DNA and cationic nanogels were mixed in phosphate-buffered saline and were probed by dynamic light scattering at a (N/P) ratio of 10:1. In this experiment, the nanogels and DNA−nanogel complexes contributed to the majority of the scattered intensity, while the concentration of DNA was too low to contribute to the scattered intensity. This allowed measurement of the nanogel and DNA−nanogel complexes without significant interference from DNA not associated to the nanogels. The measured sizes, size ranges, and diffusion coefficient ratios of the nanogel/DNA complexes are reported in Table 4.

Since there was not a significant increase in size, polydispersity, or scattered intensity between nanogels complexed to 24 bp DNA and nanogels without DNA, the nanogel−24 bp DNA complexes most likely consisted of individual nanogels complexed to one or multiple oligonucleotides. If this is the case, then an individual nanogel must possess the amount of surface charge needed to condense one or multiple 24 bp oligonucleotides. Additionally, when analyzed after 1 month at ambient temperature these complexes remained stable, with no increase in size or polydispersity.

The complexes formed with 1000 bp at (N/P) ratios of 10:1, however, were polydisperse and exhibited a large increase in scattered intensity, suggesting that, during the condensation process, the 1000 bp DNA binds to multiple nanogels, resulting in nanogel aggregation, and the large mass and polydispersity of the aggregates produced an increase in scattered intensity. The aggregation of the DNA complexes was found to be reversible by the addition of 1 M salt. When 1 M NaCl was added, the scattered intensity, diffusion coefficient ratio, and size decreased and became equivalent to nanogels in 1 M NaCl, indicating dissociation of the complexes. The dissociation of the 1000 bp complexes at 1 M NaCl, observed by light scattering, was in agreement with the dissociation of oligonucleotide complexes at 1 M salt as analyzed by size exclusion chromatography and reported in Figure 7. The aggregation of DNA complexes were also investigated by AFM, to determine if the aggregates detected by dynamic light scattering could also be observed by AFM.

Figure 8 depicts amplitude and height micrographs of nanogel−1000 bp DNA complexes deposited on the surface of silicon 111. In this AFM experiment, the surface of silicon 111 was utilized instead of mica, to avoid the negatively charged surface of mica which may have interfered with the electrostatic binding of DNA and nanogels.[73]

In these micrographs, the nanogels and DNA are absorbed onto the surface of silicon. The nanogels are surrounded and linked by single strands of DNA. Although the images of the nanogel−DNA complexes absorbed unto the silicon surface may not be an exact representation of the true morphology of the complexes in solution, the AFM images illustrate that single DNA strands link multiple nanogels and the resulting complexes are polydisperse.

The AFM micrographs in Figure 8 suggest that DNA is adsorbed onto the surface of the nanogels. These experiments, however, did not fully probe whether the DNA remained only at the surface or also penetrated into the interior of the cationic nanogels. Assuming uniform distribution of the crosslinker, the average mesh size of the cationic nanogels in aqueous solvents was estimated to range from 2 nm for nanogels containing 50 wt % crosslinker to 12 nm for nanogels containing 3 wt % crosslinker. Although the mesh size exceeded the diameter of double-stranded DNA (i.e., 2 nm), the diffusion of DNA through the network, however, may be hindered by the electrostatic interactions between the negatively charged DNA and the quaternary ammonium ions within the nanogel, causing the binding of DNA to be confined onto the surface. The distribution of DNA within the nanogel−DNA complexes is a subject for future investigations.

The nanogels investigated in the present study may possess utility for delivery of small oligonucleotides, based on the low polydispersity, small size, and excellent stability of oligonucle-

(73) Rivetti, C.; Guthold, M.; Bustamante, C. *J. Mol. Biol.* **1996**, *264*, 919−932.

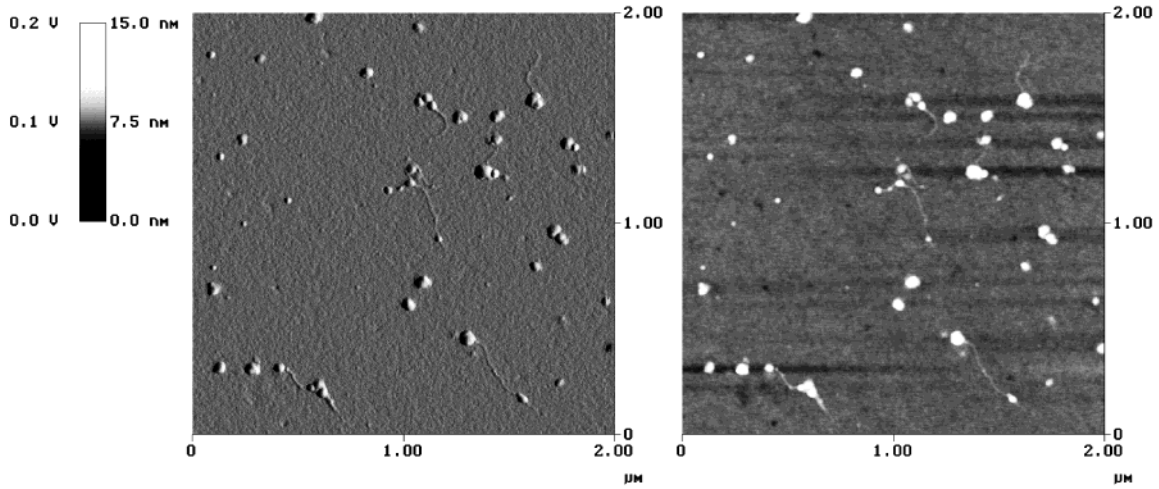

Figure 8. AFM micrographs of nanogels (50:25:25 PEGdiA:AETMAC:HEA) complexed to DNA on the surface of silicon 111. Nanogel concentration = 5 μg/mL. DNA concentration = 0.5 μg/mL. (N/P) ratio of 4:1. (Left) Amplitude micrograph: image = 2 μm^2, amplitude bar = 0.2 V. (Right) Height micrograph: image = 2 μm^2, height bar = 15 nm.

otide complexes. For delivery of larger DNA, however, nanogels with higher surface charge or greater (N/P) ratios are presumably required to promote monodisperse condensation.

Toxicity Studies. Cell viability studies were conducted to evaluate the toxicity of the nanogels. Many high molecular weight positively charged polyelectrolytes, such as polyornithine, polylysine, and polyarginine, have exhibited cyctotoxicity in cell culture.[41,74] Toxicity of these polyelectrolytes is thought to result from disruptive interactions between the polyelectrolyte and phospholipid membrane.[41] Although the cationic nanogels prepared with 25 wt % AETMAC have enough surface charge to complex DNA at physiological ionic strength, they did not induce cell death when incubated with cultured HeLa cells for 40 h. Cell survival was quantified by an MTS assay and a dye exclusion assay after the nanogels were incubated with HeLa cells. The MTS assay is based on a modified MTT assay and measures the reduction of a MTS tetrazolium compound to formazan, which correlates to percentage of living cells.[75,76] The dye exclusion assay measures cell survival by determining the percentage of cells that exclude the dye trypan blue. Figure 9 summarizes the results of both cell viability studies, and demonstrates that both the nonionic and the cationic nanogels did not significantly induce cell death compared to the blank control cells not dosed with nanogels. In addition, no significant difference in toxicity was observed for samples containing equivalent AETMAC concentrations but different PEGdiA concentrations, data not shown. On the basis of the initial toxicity data, the nanogels appear biocompatible and suitable for future in vivo investigations.

Uptake in Cell Culture. In the current investigation, confocal laser scanning microscopy was employed to measure the uptake of the nanogels in cell culture and to determine the ability of the nanogels to enhance oligonucleotide uptake. In the confocal studies, two different fluorescent probes, rhodamine and fluorescein, were used to concurrently monitor the distribution of oligonucleotide and nanogels within the same cell. Cells and

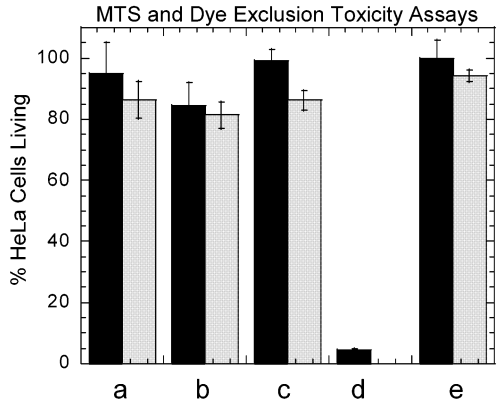

Figure 9. Toxicity study indicating % HeLa cells living after incubation with nanogels. Solid bar = MTS assay (16 h incubation at 0.125 mg/mL), crosshatched bar = dye exclusion assay (40 h incubation at 0.25 mg/mL). Nanogel samples contain 12 wt % PEGdiA with 0 wt % AETMAC (a), 12 wt % AETMAC (b), and 25 wt % AETMAC (c). Positive control: polylysine (d). Negative control: blank (e).

images were processed under identical instrumental conditions to enable direct visual comparison between cellular rhodamine and fluorescein levels.

Nanogel Uptake. To determine the cellular uptake of the nanogels, rhodamine-labeled nanogels (25 μg) were incubated for 24 h on HeLa cells (2×10^4 cells/well). After removing the unbound nanogels by washing the cells with phosphate-buffered saline, confocal images were acquired on fixed HeLa cells under rhodamine excitation. The uptake of the nanogels by HeLa cells appeared to depend on the charge concentration in the nanogel and correlated to the DNA binding studies. Uptake was only observed in samples incubated with cationic nanogels. Table 5 summarizes the uptake levels of the nanogel samples tested in HeLa cells. Uptake levels were assessed qualitatively by visually comparing the fluorescence in the sample compared to the fluorescence in a blank control.

The uptake levels were found to increase with increasing concentration of AETMAC. This may be attributed to the cationic nanogels having increased interaction with the negatively charged cell membrane surface and is in accordance with other literature reports for the uptake of positively charged macromolecules.[3]

(74) Zauner, W.; Ogris, M.; Wagner, E. *Adv. Drug Delivery Rev.* **1998**, *30*, 97−113.
(75) Cory, A. H.; Owen, T. C.; Barltrop, J. A.; Cory, J. G. *Cancer Commun.* **1991**, *3*, 207.
(76) Carmichael, J.; DeGraff, W. G.; Gazdar, A. F.; Minna, J. D.; Mitchell, J. B. *Cancer Res.* **1987**, *47*, 926−942.

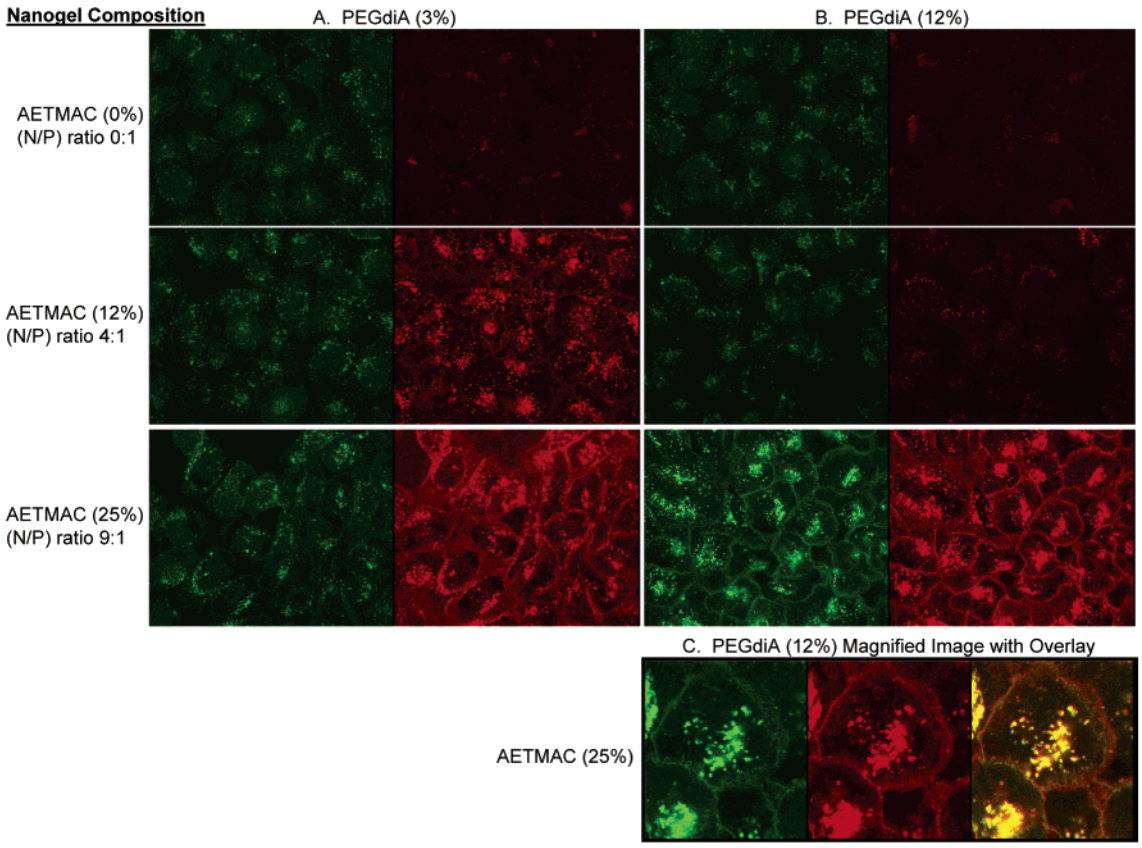

Figure 10. Confocal laser scanning micrographs of HeLa cells incubated with rhodamine-labeled nanogels and fluorescein-labeled phosphorothioate oligonucleotides. Columns and rows are labeled with PEGdiA and AETMAC (wt %) concentrations in the nanogels. Sections A and B: Right field images represent HeLa cells under rhodamine excitation; left field images represent HeLa cells under fluorescein excitation. (A) HeLa cells incubated with nanogels containing 3 wt % PEGdiA. (B) HeLa cells incubated with nanogels containing 12 wt % PEGdiA. Section C: Magnified sample of HeLa cells with 12 wt % PEGdiA and 25 wt % AETMAC. Right image represents overlay of rhodamine and fluorescein fluorescence; middle image represents rhodamine fluorescence; left image represents fluorescein fluorescence.

Table 5. Summary of Relative Uptake Levels of Nanogels in HeLa Cells: No Uptake (−), Slight Uptake (+), and High Uptake (+ +)

nanogel composition	PEGdiA (3 wt %)	PEGdiA (12 wt %)
AETMAC (0 wt %)	−	−
AETMAC (12 wt %)	+	−
AETMAC (25 wt %)	+ +	+ +

Oligonucleotide Uptake. The ability of the nanogels to facilitate oligonucleotide uptake was assessed in cultured HeLa cells using rhodamine-labeled nanogels and fluorescein-labeled 18-mer phosphorothioate oligonucleotides. Cell culture medium containing oligonucleotides (1 μM) and nanogels (25 μg) varying in composition was incubated with cultured HeLa cells (2×10^4 cells/well) for 24 h, and fixed cells were viewed by confocal laser scanning microscopy after first washing the cells with phosphate-buffered saline. Figure 10 presents the confocal images of HeLa cells under rhodamine and fluorescein excitation. The confocal studies of nanogels, with and without the presence of oligonucleotide, qualitatively exhibited similar nanogel uptake levels, indicating that the presence of oligonucleotide did not significantly alter nanogel uptake levels. The oligonucleotide uptake was significantly enhanced by the addition of nanogels prepared with 25 wt % AETMAC, while nanogels prepared with 0 and 12 wt % AETMAC did not enhance oligonucleotide uptake compared to the uptake of free oligonucleotide.

Since the nanogels prepared with 0 and 12 wt % AETMAC did not form complexes at physiological ionic strength with oligonucleotides, they were not expected to form complexes in cell culture media and promote uptake. The complexes formed with nanogels containing 25 wt % AETMAC, however, remained stable under physiological conditions, according to the chromatography studies, and thus were expected to remain stable in cell culture media and promote uptake through increased interaction with the cell membrane. If these complexes remained stable during cell membrane binding and entry, then the confocal images should display colocalization of the fluorescence from the rhodamine-labeled nanogels and the fluorescein-labeled oligonucleotide. Figure 10C illustrates the colocalization of the rhodamine and fluorescein fluorescence in HeLa cells containing oligonucleotides and nanogels prepared with 25 wt % AETMAC and 12 wt % crosslinker. The yellow in Figure 10C represents the overlay of the fluorescein and rhodamine signals, indicating that the nanogels and oligonucleotides are colocalized in the cells. These initial studies suggest that the cationic nanogels with 25 wt % AETMAC were able to enhance cellular uptake of the oligonucleotide.

Conclusions

This investigation effectively demonstrates that inverse microemulsion polymerization can be utilized to produce monodisperse, nontoxic, nanogels capable of forming stable oligonucleotide complexes and enhancing cellular delivery of oligonucleotides in vitro. This technique provided control over

the nanogel composition, size, and swelling behavior by varying the crosslinker and charged monomer concentrations in the polymerization. The nanogels synthesized in the present study were within the desired size range for gene and antisense delivery applications, and exhibited low toxicity to HeLa cells. In addition, upon extended storage, the nanogels were resistant to aggregation, exhibiting no change in size or polydispersity.

The formation and stability of nanogel−DNA complexes was influenced by both the surface charge on the nanogel and the ionic strength of the solution. Because the cationic nanogels were able to form monodisperse, stable complexes with oligonucleotides, these systems possess immediate application for antisense delivery. For gene delivery applications, however, the nanogels with increased surface charge capable of promoting monodisperse condensation of genes will need to be synthesized. Studying the in vivo distribution of these materials, adding surface cell-targeting ligands, and designing controlled release and nuclear uptake capabilities will be the subject of future investigations.

Experimental Section

Inverse Microemulsion Polymerization. Nanogels were synthesized via inverse microemulsion polymerization of the following acrylate monomers: poly(ethylene glycol) (*n*) diacrylate $n = 400$ (MW 610 g/mol, CAS Registry Number 17831-71-9), 2-hydroxyethylacrylate (CAS Registry Number 818-61-1), and 2-acryloxyethyltrimethylammonium chloride (80% solution in water) (CAS Registry Number 44992-01-0). Monomers, obtained from Polysciences, Inc., were used as received. Polymerizations were carried out in 8 mL borosilicate reaction vials using reagent grade heptane, HPLC grade water, laureth-3, and ethylhexylperoxydicarbonate (Trigonox EHP) which were obtained from Mallinckrodt, Fisher, Heterene, Inc., and Akzo Nobel, respectively. The surfactant, laureth-3, is a 12-carbon alkyl chain with an average degree of ethoxylation equal to 3 (CAS Registry Number 9002-92-0).

Microemulsion stock solutions were prepared by weighing 10 g of heptane, 1.12 g of laureth-3, and 0.4 g of an aqueous monomer stock solution into a 20 mL borosilicate glass vial followed by shaking vigorously until a one-phase optically transparent solution was obtained. Aqueous monomer stock solutions were prepared by diluting monomers with water to a final concentration of 50 wt % monomer. When the microemulsions reached equilibration, 4.61 g of the microemulsion stock was added to the reaction vial through a 0.22 μm PTFE syringe filter. The vials were sealed with silicone−Teflon lined septa, equipped with magnetic stir bars, and dissolved oxygen was removed via an argon purge while stirring at room temperature. A sample of 100 μL of initiator stock solution was added to each reaction vial during the argon purge. The initiator stock solution was prepared by adding 0.5 mL of 95% ethylhexylperoxydicarbonate to 1 g of heptane, and was stored on dry ice until used. During the polymerization, the reaction vials were stored at room temperature, under an argon atmosphere, and were protected from light for 12 h.

Synthesis of Rhodamine-Labeled Nanogels. Rhodamine-labeled nanogels were synthesized via inverse microemulsion polymerization following the same procedure described above except that microemulsions were formed with aqueous monomer solutions containing the added monomer, methacryloxyethyl thiocarbamoyl rhodamine B (Polysciences, Inc.), at a concentration of 0.25 wt % with respect to total monomer.

Purification of Nanogels. Nanogels were extracted from the polymerized microemulsions and dialyzed into water. For the extraction procedure, 3 mL of the polymerized microemulsion was added to a 15 mL centrifuge tube containing 4 mL of water and 7 mL of heptane. The tube was centrifuged for 15 min at 5000 rpm. The aqueous layer was collected, and an additional 4 mL of water was added to the tube. After repeating the centrifugation, the combined aqueous layers were washed and centrifuged three times with 1-butanol to remove laureth-3. The remaining aqueous layer was placed into a 10K molecular weight cutoff dialysis cassette (Pierce 3 mL cassettes) and dialyzed into 2 L of water for 24 h at room temperature, changing the water every 6 h. Then, the aqueous solution containing the nanogels was removed from the dialysis cassette and filtered through a sterile 0.22 μm PVDF syringe filter (Millipore) into a clean 8 mL borosilicate vial and stored at 4 °C for further characterization. The concentration of nanogels in water after dialysis was obtained by weighing the material before and after lyophilization. The approximate concentrations after purification ranged between 4 and 6 mg/mL for all samples and 50% yield was obtained.

Characterization of Nanogels and Nanogel−DNA Complexes. ^{1}H NMR spectra of microemulsion and nanogel samples were acquired on a 400 MHz Bruker NMR spectrophotometer. Light scattering measurements were performed on a spectrometer equipped with an Innova 70C 514.5 argon laser, a Brookhaven Instruments Corporation (BIC) 9000 photomultiplier connected to a BIC motor driven goniometer, and a 400 channel digital autocorrelator. Transmission electron microscopy was performed on a Philips CM 12 electron microscope equipped with a LaB6 electron gun at a voltage of 100 kV. Atomic force microscopy was performed on a Digital Instruments Multimode Scanning Probe Microscope equipped with a NanoScope computer controller in tapping mode AFM using a 10 μm scanner and with a silicon cantilever. Size exclusion chromatography was performed using 20 mL columns packed with crosslinked agarose. Electrophoresis was performed on 1% agarose gels. Cell culture studies were conducted on cell lines of cultured HeLa S3 cells expressing the IVS2-654 EGFP construct.[77] Confocal laser scanning micrographs were recorded under rhodamine and fluorescein excitation using an Olympus confocal laser scanning microscope. Sample preparation and additional instrumentation details for NMR, light scattering, TEM, AFM, electrophoresis, size exclusion chromatography, confocal laser scanning microscopy, and cell culture studies are presented in the Supporting Information.

Acknowledgment. The authors thank the Kenan family for their gracious support of K.A.M. through the establishment of the endowed William R. Kenan Jr. Distinguished Professorship in Chemistry and Chemical Engineering at the University of North Carolina at Chapel Hill and North Carolina State University. We would like to acknowledge support through an Alfred P. Sloan Research Fellowship (J.M.D.). This work was supported in part by NSF Grant DMR-0102267. Acknowledgment is also made to the donors of the ACS Petroleum Research Fund (PRF-37018-AC7) for partial support of this research.

Supporting Information Available: NMR characterization of nanogels and sample preparation and instrumentation details (PDF). This material is available free of charge via the Internet at http://pubs.acs.org.

JA027759Q

(77) Sazani, P.; Kang, S.-H.; Maier, M. A.; Wei, C.; Dillman, J.; Summerton, J.; Manoharan, M.; Kole, R. *Nucleic Acids Res.* **2001**, *29*, 3965−3974.